RSC Advances

PAPER

View Article Online
View Journal | View Issue

Cite this: *RSC Adv.*, 2015, **5**, 100838

Synthesis of bentonite clay based hydroxyapatite nanocomposites cross-linked by glutaraldehyde and optimization by response surface methodology for lead removal from aqueous solution

Piyali Roy Choudhury, Priyanka Mondal and Swachchha Majumdar*

Received 9th September 2015
Accepted 5th November 2015

DOI: 10.1039/c5ra18490h

www.rsc.org/advances

A novel nanocomposite (BT–HAp) was developed by chemical synthesis using hydroxyapatite nanoparticles and bentonite clay and was further applied for toxic lead (Pb) removal from aqueous solution. Three types of bentonite clay based nanocomposites were prepared by varying the pH of the solution (3, 7 and 10) with the addition of glutaraldehyde as a cross-linking agent. The formation and performance of the prepared BT–HAps are described herein. Clear and sharp XRD peaks suggested the presence of hydroxyapatite and bentonite clay compounds in the composite. The FTIR spectra confirmed the existence of the functional groups required to develop the nanocomposite. The Bt–HAp nanocomposites were also characterized in terms of BET, FESEM and TEM *etc.* to establish their formation. The nanocomposite synthesized at pH 7 showed a higher sorption capacity than those at pH 3 and 10. A mathematical and statistical optimizing technique (response surface methodology) was applied to verify the interactive effects of various parameters on the sorption capacity. The analysis of variance was discussed for the factors and response and confirmed the significance of the predicted model (R^2 = 0.9906). The Langmuir isotherm model best represented the phenomenon having a sorption capacity of 346 mg g^{-1} at 30 °C. The sorption mechanism was well described by the pseudo 2nd order kinetic model indicating the coexistence of both physisorption and chemisorption. Moreover, a considerable amount of toxic Pb (~99%) removal was observed for the synthesized nanocomposite *via* sorption.

1. Introduction

The application of nanoparticles for contaminated water treatment has gained remarkable interest from the scientific community recently. Metal oxide nanoparticles like Al_2O_3, MnO_2, MgO and TiO_2 were used for heavy metal removal from aqueous systems.[1] Similarly, silver nanoparticles also gained considerable attention due to their antimicrobial activity.[2] Simeonidis *et al.* (2015) found that Fe magnetite nanoparticles (20 nm) were able to remove toxic chromium from drinking water.[3] The removal capacity of Cr by the magnetic nanoparticles was 1.8 μg Cr(VI) mg^{-1} for a residual concentration of 50 μg L^{-1} at neutral pH.[3] However, these nanoparticles have some disadvantages in terms of the separation period and the reusability of nanoparticles from treated water.[4–7] Therefore, it is of utmost importance to overcome these drawbacks to produce clean water. Composite materials have gained considerable research attention in recent years for the removal of toxic contaminants from aqueous systems. These materials are easily separable from filtered water due to their comparatively large size. Nanocomposites consist of two or more components, having at least one with nano-dimensions, and have different chemical and physical properties to their individual components. The development of nanocomposites in combination with nanoparticles (NPs) having superior properties, *e.g.* large surface area, surface reactivity and high response to mechanical stimuli, could be a possible solution to the disadvantages associated with nanoparticles.[8,9]

A significant threat occurs to the environment and public health due to the discharge of heavy metals, especially Pb from printing and textile industries or other sources, into bodies of water.[10] It can cause structural damage in the mammalian eye, central nervous system and blood cells.[11] Adsorption is a widely used method for heavy metal remediation due to its simple and economic operation process compared to other conventional methods. In this context, Pb adsorption by nanocomposites could be a feasible way to remediate toxic elements from aqueous solution.[12–17]

The incorporation of natural and synthetic nanomaterials into other functional groups to form a desired nanocomposite with significant performance has gained attention nowadays. Several clay based nanocomposites containing nanoparticles

Ceramic Membrane Division, CSIR-Central Glass and Ceramic Research Institute, 196, Raja S. C. Mullick Road, Kolkata–700 032, India. E-mail: swachchha@cgcri.res.in; Fax: +91 33 2473 0957; Tel: +91 33 2473 3252

are reported for the removal of water contaminants. Chao *et al.* (2015) reported that the adsorption characteristics are strongly influenced by the bentonite clay and the metal oxide nanocomposite.[18] A new nanocomposite was developed from acid activated clay to study the adsorption feasibility of crystal violet dye.[19] Bentonite clay composite materials are now widely applied in water purification systems including heavy metal adsorption, rather than for *in situ* applications, due to the improved sorption time, efficiency and life cycle.[19–23] A bentonite clay based hydroxyapatite nanocomposite has not been reported before now, although Kanno *et al.* (2014) suggested that hydroxyapatite may be an alternative approach for the removal of toxic contaminants.[24] Very recently, the synthesized hydroxyapatites have been combined with metal oxide nanoparticles for potential application in water purification.[25–27]

It is well known that bentonite is a natural, low-cost clay mineral and largely available material. Therefore, in this study a new nanocomposite was developed combining bentonite with a hydroxyapatite nanomaterial (BT–HAp). The inclusion of a ceramic material such as bentonite clay improves the sorption capacity as well as the mechanical properties of hydroxyapatite. Glutaraldehyde is used as a cross-linking agent to adhere the components in the composite. Additionally, it has disinfectant properties with low toxicity and also enhances the mechanical properties of nanocomposites.[28] To the best of our knowledge, reports are not available regarding bentonite clay based hydroxyapatite nanocomposite synthesis and their application as a sorbent for Pb removal from synthetic water.

Additionally, the effect of different independent variables on the Pb sorption capacity has been optimized in this study. Central Composite Design (CCD) is considered to design the experimental data for the response surface methodology (RSM) optimization method. Moreover, the relationship of the response and independent variables such as the pH, initial Pb concentration and dosage is established by statistical analysis.

2. Experimental

2.1. Materials

Calcium nitrate tetrahydrate ($Ca(NO_3)_2 \cdot 4H_2O$) (99%), diammonium hydrogen phosphate ($(NH_4)_2HPO_4$) (99%), ammonia ($NH_3 \cdot H_2O$), glutaraldehyde and lead nitrate ($Pb(NO_3)_2$) (99%) from Merck, Germany were used. Bentonite clay was obtained from CSIR-CGCRI, Kolkata and used without further purification.

2.2. Synthesis of hydroxyapatite NPs

The HAp nanoparticle synthesis was conducted by the chemical precipitation method with some modifications.[29] In brief, according to a Ca/P ratio of 1.6 : 1, $Ca(NO_3)_2$ and $(NH_4)_2HPO_4$ were dissolved separately in 100 mL Milli-Q water. Aqueous NH_3 was used to maintain the pH of the solutions at 10. The solution of $Ca(NO_3)_2$ was added dropwise into the $(NH_4)_2HPO_4$ solution with rapid stirring (250 rpm). Gelatin was added later as an adhesive material during the precipitation. The greenish precipitate was repeatedly washed to remove impurities such as ammonia and its by-products. Subsequently, the green compact was washed with Milli-Q water several times. The solid product was oven dried at 50 °C overnight and sintered at 1200 °C for 2 h. Finally, the calcined HAp was powdered for application.

2.3. Preparation of BT–HAp nanocomposite

An equal ratio (1 : 1) of bentonite clay and the synthesized hydroxyapatite NPs was maintained for the nanocomposite preparation. Both of the solutions (50 mL) were stirred separately (250 rpm) in 250 mL beakers for 12 h. Hydroxyapatite solution was then poured into the bentonite clay solution with continuous stirring. Glutaraldehyde (6 to 100 mL) was added dropwise to the mixture as a crosslinker. Three sets of experiments were conducted at different pH values of 3, 7 and 10. The pH was adjusted using 0.1 N HCl and 0.1 N NaOH solutions. All the solutions were stirred at 250 rpm for 12 h at room temperature. A washing–centrifugation procedure was then followed to obtain a neutral supernatant. Finally, the prepared BT–HAp nanocomposite was dried at 60 °C for 2 h and powdered by grinding with a mortar and pestle. Fig. 1 shows the schematic of the nanocomposite formation process with changes of morphology. The prepared samples were stored in an airtight container for further use.

2.4. Experimental design

RSM is a well-known optimization approach that simultaneously considers several parameters at different design levels. Moreover, this mathematical and statistical modeling tool is used to achieve the desired product with a lower number of experiments without the requirement of observing all probable combinations experimentally.[30–34] Central composite design was undertaken to establish the relationship between the independent variables with the response of the Pb sorption capacity. Two levels with three factors (2^3) were employed in a series of experiments. Design Expert software was also used to express the regression

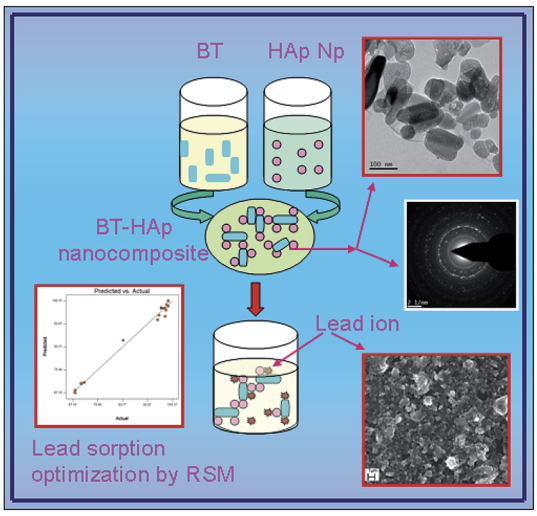

Fig. 1 Schematic of the nanocomposite preparation process with changes in morphology.

Table 1 Experimental range and levels (coded)

Independent variable	Factor code	Range and level (coded) −1	0	+1
Dose, g L^{-1}	A	0.5	1	1.5
Initial Pb concentration, mg L^{-1}	B	50	100	150
pH	C	4.5	5	5.5

model and graphical analysis of the data. A coded level (−1, 0, +1) of variables, *viz*. nanocomposite dosage 0.5–1.5 g L^{-1} (A), initial Pb concentration 50–150 mg L^{-1} (B) and initial solution pH 4.1–6.1 (C), was designed by CCD to study their effects on the sorption capacity (Table 1).

The quadratic model was designed by CCD and the response variables were expressed as a function of the process variables. In this method, a set of twenty experiments were conducted (Table 2). The quadratic model for the optimum value calculation is represented below:

$$Y = \beta_0 + \sum_{i=1}^{k} \beta_i x_i + \sum_{i=1}^{k} \beta_{ii} x_i^2 + \sum_{i=1} \sum_{j=i+1} \beta_{ij} x_i x_j \quad (1)$$

where β_0 is constant, β_i, β_{ii} and β_{ij} are regression coefficients and x_i and x_j denote the independent variables. The predicted response is represented as Y.[35]

In this study, the independent given variables were considered to be the pH, initial Pb concentration and nanocomposite dosage, whereas the sorption capacity was a dependent experimental response.

2.5. Material characterization

The X-ray diffraction (XRD) analysis of the BT–HAp nanocomposite was performed using a Philips 1710 diffractometer with Cu as the anode (Netherlands). The morphology of the powdered sample was investigated using field emission scanning electron microscopy (FESEM, Gemini Zeiss Supra™, 35 VP Model, Germany). Moreover, qualitative energy dispersive X-ray spectroscopy (EDX, Leo S430I, UK and Carl Zeiss, ΣIGMA-Germany) was used to detect the elements present in the samples. Various functional groups were detected by Fourier transform infrared spectroscopy (FTIR, Perkin-Elmer, USA). The surface area was measured by the adsorption–desorption of nitrogen using the multipoint Brunauer–Emmett–Teller (BET) method with Quantachrome (USA). Transmission electron micrographs (TEM, Technai G2 30ST-FEI, USA) and the particle size distribution of the synthesized materials (Zetasizer, Nanoseries, Malvern) were also used to understand the nature of the synthesized powder. The solution pH was measured using a pH meter (EUTECH, India). After the adsorption processes, the Pb contaminated nanocomposites were also characterized to identify any changes of functional groups or morphology.

2.6. Lead adsorption experiments

The adsorption study was carried out in batch mode. All solutions were prepared using ultrapure water from the Millipore-Q (USA) system. The synthetic solutions at different concentrations were prepared by diluting the standard Pb solution (1000 mg L^{-1}) obtained by dissolving $Pb(NO_3)_2$ quantitatively in Milli-Q water at room temperature. A sample of 10 mL volume was collected at different initial concentrations with a nanocomposite dose of 1 g L^{-1}. Adsorption studies were performed in

Table 2 2^3 factorial design matrix and experimental response as sorption capacity (mg g^{-1})

Run	A: dose	B: initial Pb conc.	C: pH	Response: sorption capacity, actual value	Response: sorption capacity, predicted value
1	0.50	50.00	4.50	98	94.78
2	1.00	156.00	5.00	68	68.10
3	1.50	50.00	5.50	99	98.46
4	0.50	50.00	5.50	98.5	99.05
5	1.50	150.00	5.50	70	70.59
6	1.00	100.00	5.00	97	97.72
7	1.50	50.00	4.50	99	100.25
8	1.00	100.00	5.00	96.7	97.72
9	1.84	100.00	5.00	98.2	96.96
10	1.00	100.00	5.84	96	95.15
11	1.00	100.00	5.00	97.5	97.72
12	0.20	80.00	4.00	84	86.09
13	0.50	150.00	4.50	68	67.16
14	1.50	150.00	4.00	70	70.5
15	1.00	100.00	5.00	98	97.72
16	1.00	50.00	5.00	99	100.37
17	1.00	100.00	5.00	97.3	97.72
18	1.00	100.00	5.00	97.5	97.72
19	1.00	100.00	4.16	95.5	93.52
20	0.50	150.00	5.50	71	70.88

a batch reactor at 250 rpm using a magnetic stirrer for 24 h. The pH, nanocomposite dosage and initial Pb concentration variations were conducted for efficient Pb sorption studies. In addition, the Pb sorption was carried out at different temperatures to observe the effect on the removal efficiency. The concentration of Pb was measured by ion chromatography (881 Compact IC pro, Metrohm). A repeatability study was carried out for all experiments and the errors were found to be minimal. The sorption capacity q_e (mg g^{-1}) and removal efficiency (R) were calculated from the following equations:

$$q_e = V(C_0 - C_e)/m \quad (2)$$

$$R = (C_0 - C_e)/C_0 \times 100 \quad (3)$$

where V is the volume of the solution (L), C_0 and C_e are the initial and equilibrium Pb concentration (mg L^{-1}) and m (g) is the mass of the nanocomposite as adsorbent.

2.7. Desorption study

The desorption study was accomplished in batch mode with 0.1 M ethylenediaminetetraacetic acid (EDTA), NaOH and HNO_3. The other conditions remained unchanged and about 0.01 g of spent nanocomposite was taken for each solution. A desorption study was carried out at 250 rpm for 180 minutes at 30 °C. The desorption efficiency was estimated from the following standard equation:

$$\%\ \text{desorption} = C_d/C_a \times 100 \quad (4)$$

where C_d and C_a are the amount of metal ions desorbed and adsorbed in mg L^{-1}.

3. Results and discussion

3.1. Characterization of nanocomposites

The XRD patterns of the BT–HAp nanocomposites are shown in Fig. 2(a–c). The crystal phase obtained by XRD analysis clearly shows an increase in crystallinity for the BT–HAp nanocomposite at pH 7 (Fig. 2(b)) compared to BT–HAp at pH 3 and 10 (Fig. 1a and c). This result demonstrated the highly crystalline structure of BT–HAp-7. The sharp and major peaks related to HAp were observed at 25.94, 29.02, 31.89, 32.28, 33.0, 34.15, 39.93, 49.6 and 53.3 at 2θ degrees. The positions and d-values matched well with JCPDS no. 09-0432.[26] However, the peaks at 2θ = 5.3, 24.5, 34.7 and 63.2 confirmed the presence of bentonite clay in the composite. Similar findings were reported previously by T. S. Anirudhan *et al.*, 2006.[36] Therefore, the formation of the nanocomposite BT–HAp was corroborated by XRD analysis. The crystallite size was estimated by Scherrer's equation from the XRD pattern, $D = \kappa\lambda/\beta \cos\theta$, where the constant κ is 0.9–1, λ is the X-ray wavelength, β is the full-width half maximum and θ is the Bragg's angle. The crystallite sizes of BT–HAp-3, 7 and 10 were 28.6 nm, 36.7 nm and 45.9 nm, respectively.

In Fig. 3, the FTIR spectra a, b and c correspond to the synthesized nanocomposites BT–HAp-3, -7, and -10. The

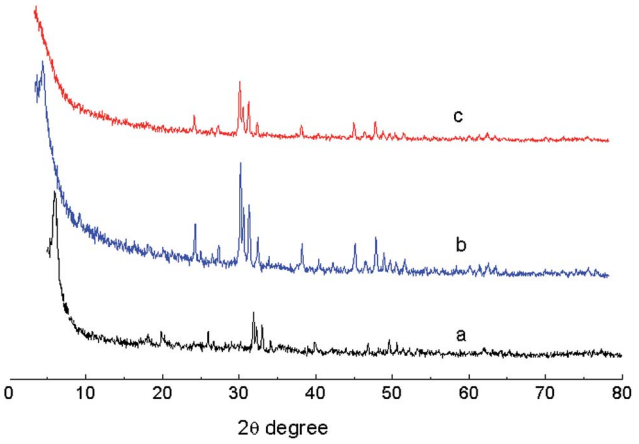

Fig. 2 XRD patterns of the nanocomposites for BT–HAp at (a) pH 3, (b) pH 7 and (c) pH 10.

functional groups of the composite material were present in the above-mentioned three types of nanocomposite with variation of the transmittance. The absorption bands at 3627–3630 cm^{-1} were assigned to the hydroxyl group (–OH). The broad absorption bands at 3434 and 1633 cm^{-1} may be attributed to the –OH stretching and bending, respectively for the adsorption of water molecules on the clay and hydroxyapatite surfaces. The chemical cross-linker glutaraldehyde helped to attach the active groups (*e.g.* aldehyde) of the HAp particles or clay mineral to each other.[37] Absorption bands at 1040–1044 cm^{-1} signify the presence of Si–O–Si bonds in BT–HAp. Additionally, another form of silica was observed at 522–527 cm^{-1} for the BT–HAp nanocomposites prepared at pH 3, 7 and 10. The presence of the typical vibrations of 6-membered rings combined with alumina and silica-oxygen tetrahedral groups are at 633 cm^{-1}.[38] The $-PO_4$ characteristic groups were assigned to the absorption band at 1036–1043 cm^{-1} which confirms the presence of hydroxyapatite in the BT–HAp nanocomposite. In addition, the

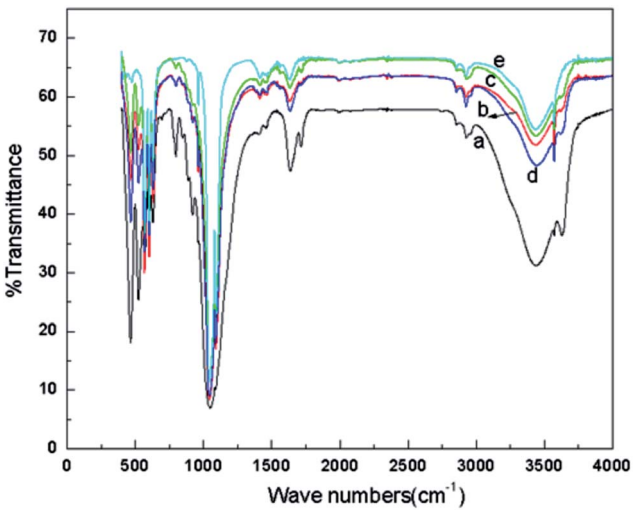

Fig. 3 FTIR spectra of the nanocomposites for: (a) pH 3, (b) pH 7, (c) pH 10, (d) after sorption and (e) HAp NPs.

occurrence of hydroxyapatite in the nanocomposite may be verified by its absorption band in the FTIR spectra. Thus, the above observation clearly indicates the formation of the BT–HAp nanocomposite. After the sorption of Pb, the intensity was shifted and the reduced intensity of the OH^{-1} group is shown in Fig. 3(d). The change in the FTIR spectrum after Pb sorption clearly demonstrates that the Pb ions were adsorbed on the BT–HAp surface due to electrostatic attractions which signifies the physical sorption process.[39] The FESEM images (Fig. 4(a–e)) describe the surface morphology of the synthesized powder before and after the sorption process. Fig. 4(a) signifies the formation of nearly uniform spherical HAp nanoparticles with the particle size of 35–40 nm. The EDX analysis associated with FESEM was very useful to detect the elemental composition of the nanocomposites. The EDX analysis (inset of Fig. 4(a)) confirmed the presence of calcium, phosphate and oxygen elements in the HAp nanoparticles. From Fig. 4(b–d) the porous surface of the nanocomposites and a particle size varying from 75–80 nm was observed. In Fig. 4(e), the micrograph reveals Pb sorption on the nanocomposite surface and this was also confirmed by EDX analysis (inset of Fig. 4(e)).

The bright field TEM images confirmed the nanocomposite size ranges from 50–80 nm with a porous surface (Fig. 5(a–c)).

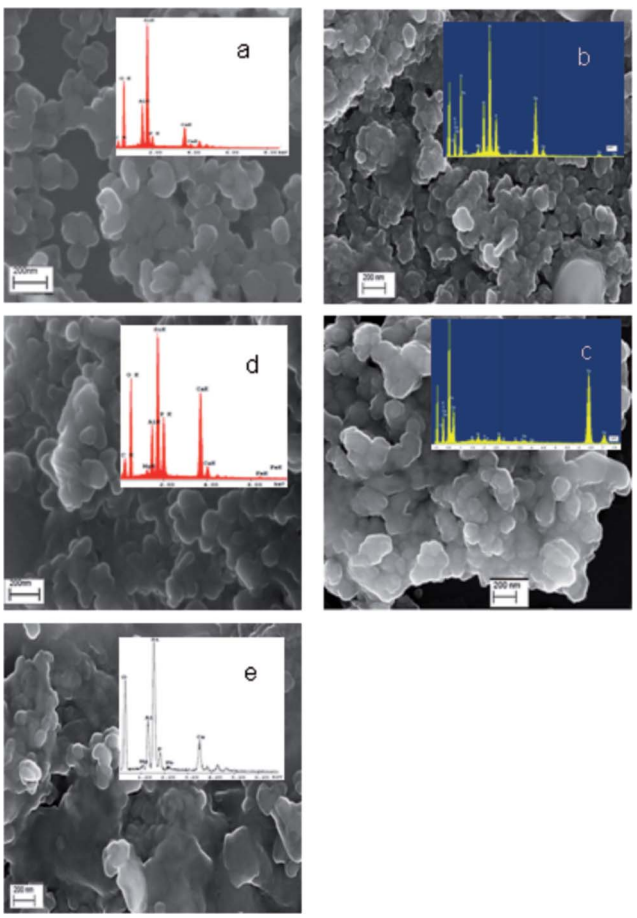

Fig. 4 FESEM and EDX spectra: (a) HAp nanoparticles, and (b) BT–HAp-3, (c) BT–HAp-7 and (d) BT–HAp-10 nanocomposites; (e) after sorption process.

The HRTEM images are presented in the inset of the TEM images of the particular nanocomposite. The interlayer spacing is equal to 0.294 nm of the BT–HAp-7 nanocomposite in the HRTEM image, corresponding to the (211) plane. From the low resolution TEM image, the characteristic crystalline spots were obtained from the SAED pattern (Fig. 5(d–f)). The diffraction rings and bright spots were due to the polycrystalline nature of the nanocomposites. Very clear rings and spots of nanoparticles suggested the formation of highly crystalline BT–HAp-7 (Fig. 5(e)). A similar observation was also made from the XRD pattern.

The surface area was measured by absorption–desorption of nitrogen by the multipoint BET method. Further chemical treatment was not performed. The samples were degassed at a temperature of 200 °C for 2 h followed by flushing with helium gas. The moisture content and unwanted air was removed from the pores of the samples by helium degassing. The relative pressure was maintained in the range of 0.05–0.3 to measure the surface area. The surface area of BT–HAp decreased as the pH of the solution increased (pH 3 – 21.89 $m^2\ g^{-1}$, pH 7 – 12.4 $m^2\ g^{-1}$, pH 10 – 11.9 $m^2\ g^{-1}$) and therefore, the maximum surface area was obtained for BT–HAp-3. However, the particle size of the nanocomposites behaves inversely to the surface area and it increased with increasing solution pH. The crystallite size is also observed earlier in the same pattern. The average pore diameter and pore volume was determined by the Barrett–Joyner–Halenda (BJH) method. It was observed that the pore diameter and pore volume were much higher (*e.g.* BT–HAp-7: 522.9 Å and 0.1627 $cm^3\ g^{-1}$) which plays a significant role for the sorption of metal ions. From the intensity *vs.* particle diameter plot, it was observed that the average particle size (d_{50}) of the nanoparticles was around 100 nm.

3.2. Response surface optimization: ANOVA result

According to the design matrix by CCD, ANOVA results from the software are listed in Table 3. A quadratic regression model equation describing the sorption process resulting from the ANOVA study can be expressed as follows:

$$\begin{aligned}\text{Sorption capacity} = {} & +97.72 + 1.29A - 13.87B + 0.48C - 1.04A^2 \\ & - 11.23B^2 - 1.2C^2 + 0.074AB \\ & - 1.51AC - 0.14BC \end{aligned} \quad (5)$$

The above regression model shows the relation between the response and the independent variables in terms of the coded factor. It can be predicted from the equation that the dosage and solution pH has a positive effect on the adsorption and the initial Pb^{2+} concentration has a negative effect on the sorption capacity. The highest order of the significant effect by the different independent variables and their interactions on the sorption capacity is B and the lowest is AB. An ANOVA study was performed to justify the significance of the quadratic model. The model *F*-value of 117.34 implies the significance of the model (Table 3). There was only 0.01% possibility of noise in the predicted model. A good correlation was observed between the experimental data and the predicted data. The multiple

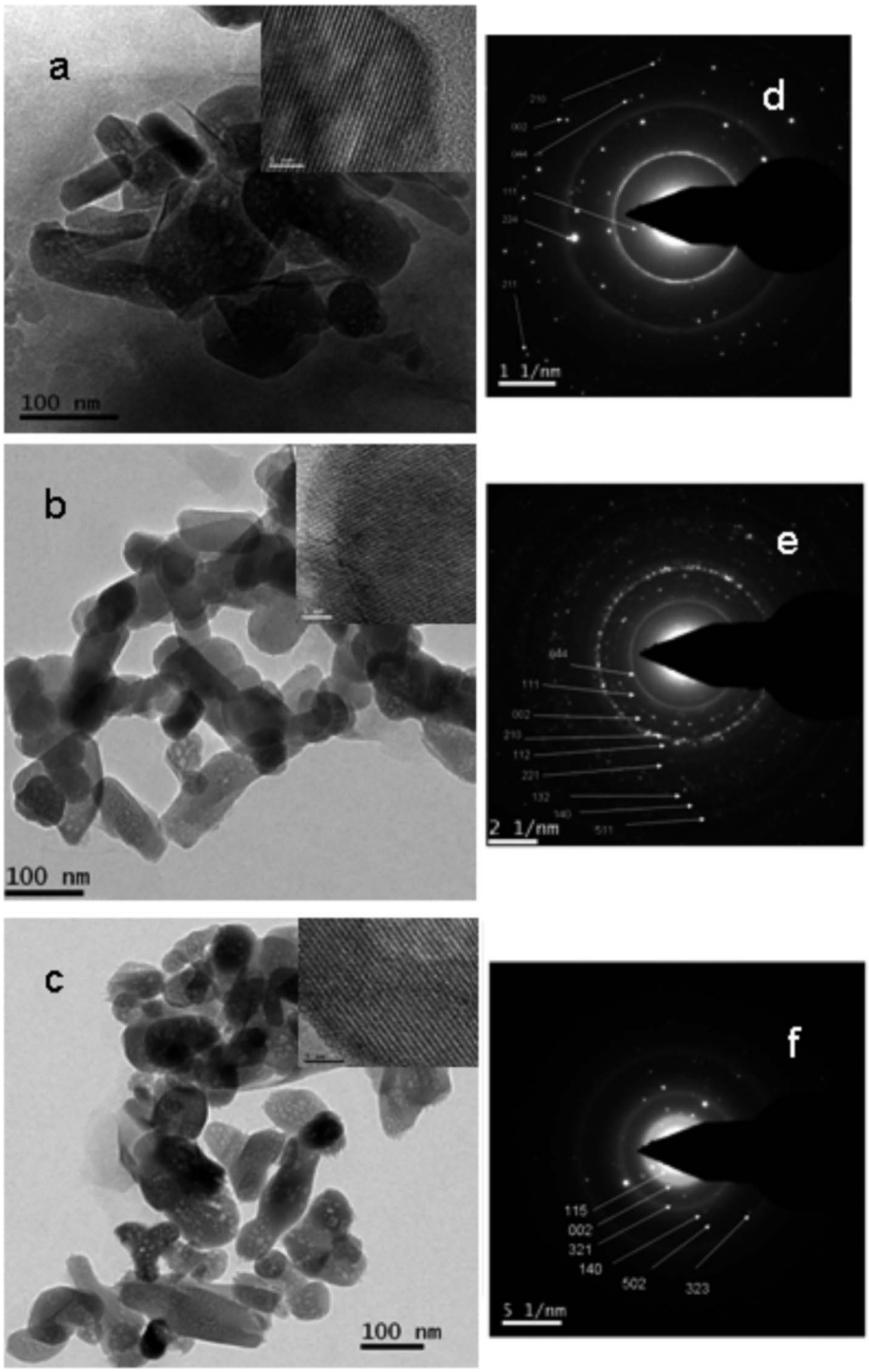

Fig. 5 TEM images of the BT–HAp nanocomposites: bright field images of (a) BT–HAp-3, (b) BT–HAp-7 and (c) BT–HAp-10 with HRTEM in the inset and (d–f) the corresponding SAED patterns.

correlation coefficient (R^2) was found to be 0.9906 which implies that 99.06% of the variations of the sorption capacity could be explained by the model. The 'Pred R^2'of 0.9051 was in logical conformity with the 'Adj R^2' of 0.9822.

3.3. Interactive effect of variables on the sorption capacity

The effect of experimental variables and the response of the sorption capacity were analyzed which was designed by CCD with a full factorial based on three factors. Table 4 represents a comparative study on the Pb sorption capacity of the nanocomposites and their basic components with 100 mg L^{-1} initial Pb solution at pH 7. The maximum sorption capacity was found for the BT–HAp-7 nanocomposite (97.94 mg g^{-1}) compared to BT–HAp-3 (95 mg g^{-1}) and BT–HAp-10 (93 mg g^{-1}) as shown in Table 4. Hence, all the sorption experiments were carried out for the most promising BT–HAp-7 nanocomposite. Although

Table 3 ANOVA for the quadratic model[a]

Source	Sum of squares	Degree of freedom (df)	Mean square	*F*-value	Probability > *F*	Coefficient estimate
Model	2973.11	9	330.35	117.34	<0.0001	—
A	17.08	1	17.08	6.07	0.0335	1.29
B	1911.58	1	1911.58	679.01	<0.0001	−13.87
C	3.61	1	3.61	1.28	0.2841	0.48
AB	0.041	1	0.041	0.015	0.9059	0.074
AC	30.09	1	30.09	10.69	0.0084	−1.51
BC	0.18	1	0.18	0.062	0.8082	−0.14
A^2	9.91	1	9.91	3.52	0.0900	−1.04
B^2	575.49	1	575.49	204.42	<0.0001	−11.23
C^2	30.77	1	30.77	10.93	0.0079	−1.20

[a] $R^2 = 0.9906$, Adj $R^2 = 0.9822$, Pred $R^2 = 0.9051$.

bentonite clay (78 mg g^{-1}) and HAp nanoparticles (83 mg g^{-1}) did not show good sorption capacity individually compared to the BT–HAp nanocomposite, the combination of these two components was explored for their potential capacity. It was reported that the particle sizes influence the sorption process noticeably during the *in situ* application of nanoparticles.[40] Results show that, although the BT–HAp-7 nanocomposite has less surface area than BT–HAp-3, it has better adsorption properties than BT–HAp-3. Therefore, the particle size was not solely responsible for the sorption capacity. The Pb solution was possibly able to diffuse through the particles and a poor correlation might be obtained for the external surface, suggesting that the particle size was not the prime parameter controlling the equilibrium sorption. However, at equilibrium, the sorption capacity and specific surface area were not directly proportional to each other.[17] Fig. 6(a) reveals the combined effect of the dose corresponding to the initial Pb concentration on the sorption capacity of the nanocomposites in a contour plot. In this plot, we observed that the sorption capacity increased with increasing dosage whereas, at the same time under the equivalent experimental conditions, the sorption capacity decreased with increasing Pb concentration. The sorption capacity was reduced from 99.4 to 75% with increasing Pb concentration from 50 to 150 mg L^{-1} with 1 mg L^{-1} dose. Therefore, the metal ion uptake by the nanocomposite was reduced by the decreasing driving force in the form of the concentration gradient. On the other hand the sorption capacity was enhanced with the increasing dosage of the nanocomposite due to the attachment of Pb to the higher surface area of the nanocomposites.

Table 4 Comparative study of lead sorption capacity

Sorbent	Adsorption capacity, mg g^{-1}
BT–HAp-3	95
BT–HAp-7	97.94
BT–HAp-10	93
Bentonite clay powder	78
HAp nanopowder	83

The combined effect of the dose and the solution pH on Pb removal are shown in Fig. 6(b). It was observed that the sorption capacity increases with increasing nanocomposite dosage. It was also found by the quadratic model that the dose parameter

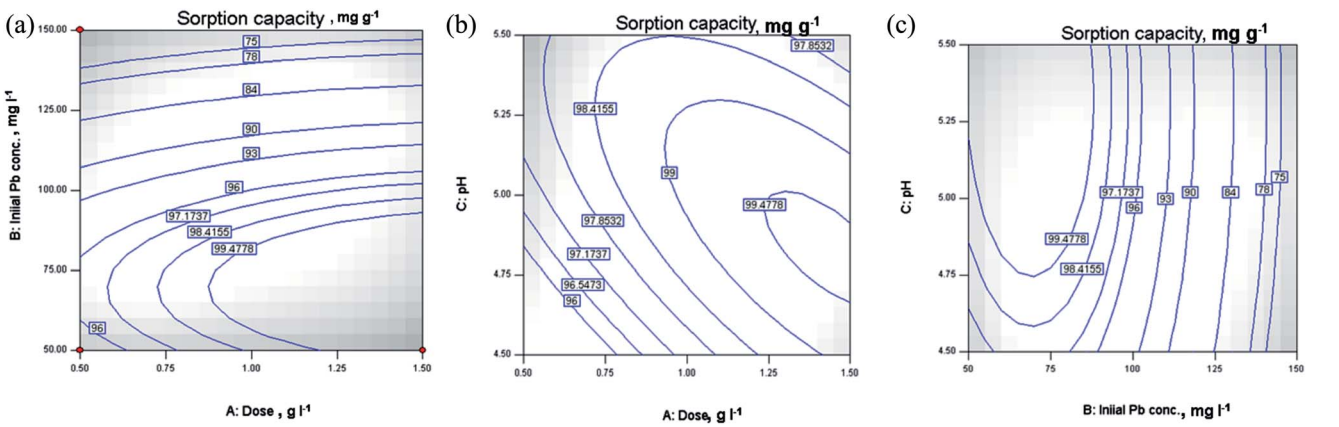

Fig. 6 Contour plots demonstrating the effect of independent variables on the sorption capacity. (a) Dose *vs.* initial Pb conc., (b) dose *vs.* pH and (c) initial Pb conc. *vs.* pH.

has a positive effect on the sorption capacity. However, a change in the sorption capacity beyond 1 g L^{-1} dose considering 100 mg L^{-1} Pb^{2+} concentration was insignificant. Therefore, the optimum dose was considered to be 1 g L^{-1} with the equivalent experimental conditions. The solution pH is an important factor that significantly influences the sorption capacity or removal efficiency. The contour plot revealed that the sorption capacity increases from 96% to 99.4% upon increasing the pH from 4.5 to 5. However, the sorption capacity decreases from 99.48 to 97.8% upon changing the pH from pH 5 to 5.5. At a lower pH (<5), the BT–HAp nanocomposite surfaces become positively charged due to the higher H^+ ion concentration, resulting in a lower sorption capacity due to repulsion between the positively charged nanocomposite surface and Pb^{2+}. The solution favored a higher sorption capacity at pH 5 due to an electrostatic attraction between the negatively charged BT–HAp nanocomposite surface and the Pb^{2+}, although beyond this pH the sorption experiment was unsuccessful due to precipitation of Pb as lead hydroxide.[41] Hence, selection of an exact pH is very important and in this study the optimum pH was found to be 5 by response surface methodology.

The pH has a positive effect on the sorption capacity (eqn (5)). Fig. 6(c) represents the collective effect of the pH and initial Pb concentration on the sorption capacity. The sorption capacity decreases from 99.4 to 75% with increasing Pb concentration from 50 to 150 mg L^{-1} by applying a 1 g L^{-1} dose at pH 5. The nanocomposites' active sites were enclosed by more Pb ions and became saturated when a higher Pb concentration was used and therefore, the sorption capacity decreased.[42] Similar observations were also found for other pH values.

3.4. Validation and confirmation of the model

Validation is a technique of RSM that is used to check the accuracy of the predicted model and the corresponding results are shown in Table 2. Assessment of the experimental test and predicted findings confirms similar responses (Fig. 7). The software was allowed to select the targeted goal for factors or responses from numerical optimization. In this study, the factors were within the range and based on the corresponding 10 optimum conditions, the sorption capacities were about 97.94 mg g^{-1} with 0.95% deviation from the experimental values. From 10 optimum conditions in the numerical optimization method, the desirability as an objective function was found to be 1 by considering the desired goals (Table 5). Therefore, the regression model successfully explained the process with high accuracy and is reliable for predicting the sorption capacity.[32]

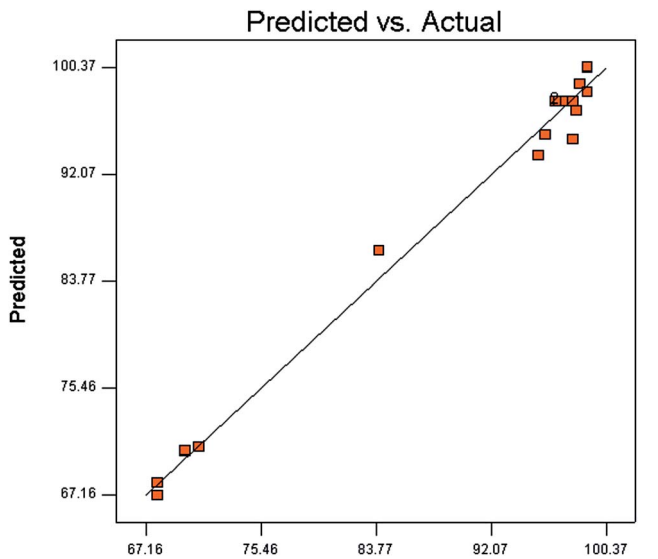

Fig. 7 Validity of the model: actual *vs.* predicted plot.

Table 5 Numerical optimization of the experiment: 10 solutions with a desirability of 1

A (dose, g L^{-1})	B (initial Pb concentration, mg L^{-1})	C (pH)	*R*1 (sorption capacity, mg g^{-1})
0.80	97.33	5.13	97.9469
1.01	149.53	4.66	72.2151
0.65	99.96	4.74	95.1846
0.53	87.31	4.77	97.2562
0.76	100.15	4.83	96.2751
0.79	98.81	5.36	97.5142
0.69	128.46	5.15	85.2497
1.34	93.27	5.43	98.4342
1.10	111.00	5.50	93.3238
0.60	94.23	5.43	98.0828

3.5. Adsorption isotherm and kinetics

A sorption capacity estimation is necessary to ascertain the amount of sorbent required for the potential removal of heavy metals such as Pb from aqueous solution. An adsorption isotherm study was conducted by varying the Pb concentration from 50 to 150 mg L^{-1} with a dosage of 1 g L^{-1} for 24 h contact time. The temperature was varied as 20, 30 and 50 °C to conduct the isotherm study.

The equilibrium data was further analyzed by the Langmuir and Freundlich isotherm models to understand the sorption behavior. The Langmuir model is based on monolayer coverage with homogeneous surface sites whereas the Freundlich model is applicable only for highly heterogeneous surfaces.[43,44] Table 6 represents the results of the isotherm model and we observed that the Langmuir model fitted well with the correlation coefficient (R^2) of 0.99. The higher n value indicates the favorable

Table 6 Langmuir and Freundlich isotherm model parameters for lead sorption

Langmuir model			Freundlich model		
R^2	q_m (mg g^{-1})	K_L (L mg^{-1})	R^2	K_F mg g^{-1} (mg $L^{-1})^n$	n
0.99	346	0.015	0.97	2.6	1.39

Table 7 Adsorption capacity of various nanocomposite

Nanocomposite	Adsorption capacity, mg g^{-1}	References
AC–HAp	9–14	M. S. Fernando *et al.*[45] DOI: 10.1016/j.apsusc.2015.05.092
SWCNTs/WSh	185.2	S. Saadat *et al.*[46] DOI: 10.1016/j.jece.2014.08.024
Poly(*o*-phenylenediamine)/ reduced graphene oxide	228	L. Yang *et al.*[47] DOI: 10.1016/j.apsusc.2014.04.083
Silica nanopowders/alginate	83.33	R. D. C. Soltani *et al.*[48] DOI: 10.1016/j.jtice.2013.09.014
BT–HAp	**346**	**This study**

conditions of the adsorbate on the sorbent surface. The Pb monolayer was bonded with the functional groups of the BT–HAp-7 nanocomposite during sorption. The maximum sorption capacity was found to be 346 mg g^{-1} and that was significantly higher compared to the other materials shown in Table 7.

Pseudo kinetic models were studied to observe the sorption mechanism. The pseudo 1st order and 2nd order kinetic models with empirical equations were used to determine the rate kinetics.[49] It was observed that the sorption capacity was very fast within the first 15 minutes but after that the process became slower before reaching equilibrium. The pseudo 2nd order model fitted best, with a linear regression correlation coefficient (R^2) value of 0.999. The rate constant (k_2) value indicated the chemisorption process of Pb ions on the nanocomposite surface.[50]

3.6. Desorption study of the nanocomposites

The adsorbents were loaded with toxic heavy metals which generates environmentally hazardous solid spent waste. Therefore, the regeneration of spent materials can make the process cost-effective. A desorption study was conducted using EDTA, HNO_3 and NaOH solution. A maximum desorption of about 64% from spent nanocomposites containing 97 mg g^{-1} of Pb was observed using EDTA solution whereas only 0.12 and 0.01% desorption was observed for HNO_3 and NaOH, respectively at 60 minutes contact time. Equilibrium was reached after 120 minutes with constant stirring. Three consecutive sorption–desorption cycles were performed and the sorption capacity of the nanocomposite decreased about 12–16% during this period. Y. Ren *et al.* (2012) hypothesized that the sorption–desorption process involved complexation, physisorption and ion exchange reactions.[50] However, the reason behind the improved desorption efficiency of EDTA solutions can be explained by the reaction of loosely bound Pb^{2+} with EDTA, that produced a stable lead acetate complex and desorbed quickly. Therefore, the nanocomposites were regenerated for further use.[51]

4. Conclusions

The nanocomposite (BT–HAp) was successfully synthesized from bentonite clay and hydroxyapatite by chemical synthesis. The novelty of this work lies in the development of three different nanocomposites from clay and HAp powder having distinguishing properties. Additionally, the novel nanocomposites can potentially be applied for toxic heavy metal (Pb) remediation. A very simple synthesis process is discussed in this report, where the raw materials are of very low-cost. Hence there is a possibility to scale-up the process in a cost-effective manner with less hazardous components. The BT–HAp nanocomposite was synthesized at neutral pH which is very significant for application in natural conditions and the minimal use of chemicals makes the process environmentally friendly. The formation of the BT–HAp nanocomposite was confirmed through XRD, FTIR, FESEM, EDX and TEM analyses. BT–HAp-7 was established as a potential sorbent having a lower surface area than BT–HAp-3. This observation indicated that the external surface was not the main parameter for sorption. The ANOVA results showed that the optimization of Pb sorption on the nanocomposites by RSM was in good agreement with the experimental results under the optimized conditions. The multiple correlation coefficient ($R^2 = 0.9906$) value also justified the above observations. The model designed by CCD describes the sorption process well, where the sorbent dose and the pH have a positive effect. However, the initial Pb concentration had a negative effect on the sorption process. The numerical optimization method showed that the Pb sorption capacity of the nanocomposites was about 97.94 mg g^{-1}. The sorption process fits well with the Langmuir isotherm model and signifies monolayer Pb sorption on the nanocomposite surface. The sorption mechanism of the nanocomposite was also well explained by the pseudo 2nd order model, which indicated chemisorption. In summary, the experimental and theoretical results suggest that the BT–HAp nanocomposite could be a potential, low-cost sorbent for heavy metal remediation from wastewater from an environmentally friendly approach.

Acknowledgements

This work was financially supported by Council of Scientific and Industrial Research, New Delhi, India.

References

1 K. Simeonidis, S. Mourdikoudis, E. Kaprara, M. Mitrakas and L. Polavarapu, Inorganic engineered nanoparticles in drinking water treatment: a critical review, *Environ. Sci.: Water Res. Technol.*, 2015, DOI: 10.1039/c5ew00152h.

2 L. Cui, P. Chen, S. Chen, Z. Yuan, C. Yu, B. Ren and K. Zhang, *In Situ* Study of the Antibacterial Activity and Mechanism of

Action of Silver Nanoparticles by Surface-Enhanced Raman Spectroscopy, *Anal. Chem.*, 2013, **85**, 5436.

3 K. Simeonidis, E. Kaprara, T. Samaras, M. Angelakeris, N. Pliatsikas, G. Vourlias, M. Mitrakas and N. Andritsos, Optimizing magnetic nanoparticles for drinking water technology: the case of Cr(VI), *Sci. Total Environ.*, 2015, **535**, 61.

4 Y. L. F. Musico, C. M. Santos, M. L. P. Dalidab and D. F. Rodriguesa, Improved removal of lead(II) from water using a polymer-based graphene oxide nanocomposite, *J. Mater. Chem. A*, 2013, **1**, 3789.

5 S. Pal, A. S. Patra, S. Ghorai, A. K. Sarkar, R. Das and S. Sarkar, Modified guar gum/SiO_2: development and application of a novel hybrid nanocomposite as a flocculant for the treatment of wastewater, *Environ. Sci.: Water Res. Technol.*, 2015, **1**, 84.

6 A. Mahapatra, B. G. Mishra and G. Hotan, Adsorptive removal of Congo red dye from waste water by mixed iron oxide–alumina nanocomposite, *Ceram. Int.*, 2013, **39**, 5443.

7 Y. Liu, c. Luo, J. Sun, H. Li, Z. Sun and S. Yan, Enhanced adsorption removal of methyl orange from aqueous solution by nanostructured proton-containing δ-MnO_2, *J. Mater. Chem. A*, 2015, **3**, 5674.

8 K. Kalpana and V. Selvaraj, A novel approach for the synthesis of highly active ZnO/TiO_2/Ag_2O nanocomposite and its photocatalytic applications, *Ceram. Int.*, 2015, **41**, 9671.

9 Y. Lu, Y. Yang, A. Sellinger, M. Lu, J. Huang, H. Fan, R. Haddad, G. Lopez, A. R. Burns, D. Y. Sasaki, J. Shelnutt and C. J. Brinker, Self-assembly of mesoscopically ordered chromatic polydiacetylene/silica nanocomposites, *Nature*, 2001, **410**, 913.

10 M. D. C. Hernández-Sariano, A. Pena and M. D. Mingorance, Environmental hazard of cadmium, copper, lead and zinc in metal-contaminated soils remediated by sulfosuccinamate formulation, *J. Environ. Monit.*, 2011, **13**, 2830.

11 A. B. G. Lansdown, in *Metal Ions Toxicology: Effects, Interactions, Interdependencies*, RSC, 2011, vol. 8, ch. 9, p. 187.

12 S. S. Samandari, S. S. Samandari, N. Nezafati and K. Yahyaa, Efficient removal of lead(II) ions and methylene blue from aqueous solution using chitosan/Fe–hydroxyapatite nanocomposite beads, *J. Environ. Manage.*, 2014, **146**, 481.

13 L. Aroui, L. Zerroual and M. Boutahalab, Synthesis and characterization of a PbO_2–clay nanocomposite: removal of lead from water using montmorillonite, *Mater. Res. Bull.*, 2012, **47**, 206.

14 S. Ghorai, A. Sinhamahapatra, A. Sarkar, A. B. Panda and S. Pal, Novel biodegradable nanocomposite based on XG-*g*-PAM/SiO_2: application of an efficient adsorbent for Pb^{2+} ions from aqueous solutions, *Bioresour. Technol.*, 2012, **119**, 181.

15 C. M. Futalan, C. C. Kan, M. L. Dalida, K. J. Hsien, C. Pascuad and M. W. Wan, Comparative and competitive adsorption of copper, lead and nickel using chitosan immobilized on bentonite, *Carbohydr. Polym.*, 2011, **83**, 528.

16 N. P. J. Jovicic, A. D. M. Nikolic, M. J. Zunic, Z. D. Mojovic, P. T. Bankovic, I. A. Grzetic and D. M. Jovanovic, Synergic adsorption of Pb^{2+} and reactive dye-RB5 on two series of organomodified bentonites, *J. Contam. Hydrol.*, 2013, **150**, 1.

17 R. Han, W. Zou, Z. Zhang, J. Shi and J. Yang, Removal of copper(II) and Pb(II) from aqueous solution by manganese oxide coated sand I. Characterization and kinetic study, *J. Hazard. Mater.*, 2006, **137**, 384.

18 C. Yanga, Y. Zhua, J. Wanga, Z. Lia, X. Sua and C. Niub, Hydrothermal synthesis of TiO_2–WO_3–bentonite composites: conventional *versus* ultrasonic pretreatments and their adsorption of methylene blue, *Appl. Clay Sci.*, 2015, **105**, 243.

19 A. A. Oladipo and M. Gazi, Enhanced removal of crystal violet by low cost alginate/acid activated bentonite composite beads: optimization and modeling using non-linear regression technique, *Journal of Water Process Engineering*, 2014, **2**, 43.

20 E. I. Unuabonah and A. Taubert, Clay–polymer nanocomposites (CPNs): adsorbent of the future for water treatment, *Appl. Clay Sci.*, 2014, **99**, 83.

21 X. Wang, L. Yang, J. Zhang, C. Wang and Q. Li, Preparation and characterization of chitosan–poly(vinyl alcohol)/bentonite nanocomposite for adsorption of Hg(II) ions, *Chem. Eng. J.*, 2014, **251**, 404.

22 M. E. Parolo, G. R. Pettinari, T. B. Musso, M. P. S. Izquierdo and L. G. Fernandez, Characterization of organo-modified bentonite sorbents: the effects of modification conditions on adsorption performance, *Appl. Clay Sci.*, 2014, **320**, 356.

23 S. S. Gupta and K. G. Bhattacharyya, Adsorption of metal ions by clays and inorganic solids, *RSC. Adv.*, 2014, **4**, 28537.

24 C. M. Kanno, R. L. Sanders, S. M. Flynn, G. Lessard and S. C. B. Myneni, Novel apatite-based sorbents for defluoridation: synthesis and sorption characteristics of nano-micro-crystalline hydroxyapatite-coated limestone, *Environ. Sci. Technol.*, 2014, **48**, 5798.

25 W. Kantana, P. Jarupoom, K. Pengpat, S. Eitssayeam, T. Tunkasiri and G. Rujijanagul, Properties of hydroxyapatite/zirconium oxide nanocomposites, *Ceram. Int.*, 2013, **39**, S379.

26 A. Farzadi, M. Solati-Hashjin, F. Bakhshi and A. Aminian, Synthesis and characterization of hydroxyapatite/b-tricalcium phosphate nanocomposites using microwave irradiation, *Ceram. Int.*, 2011, **37**, 65.

27 H. E. I. Khal and N. H. Batis, Effects of temperature on the preparation and characteristics of hydroxyapatite and its adsorptive properties toward lead, *New J. Chem.*, 2015, **39**, 3597.

28 Y. Q. Tan, Y. H. Song and Q. Zheng, Facile regulation of glutaraldehyde-modified graphene oxide for preparing free-standing papers and nanocomposite films, *Chin. J. Polym. Sci.*, 2013, **31**, 399.

29 C. Shu, Y. Xianzhu, X. Zhangyin, X. Guohua, L. Hong and Y. Kangde, Synthesis and sintering of nanocrystalline hydroxyapatite powders by gelatin based precipitation method, *Ceram. Int.*, 2007, **33**, 193.

30 G. Wang, S. Zhang, T. Li, X. Xu, Q. Zhong, Y. Chen, O. Deng and Y. Li, Application of response surface methodology for optimization of lead removal from contaminated soil using chelants, *RSC Adv.*, 2015, **5**, 58010.

31 H. Farnoush, J. A. Mohandesi, D. H. Fatmehsari and F. Moztarzadehb, A kinetic study on the electrophoretic deposition of the hydroxyapatite-titania nanocomposite based on a statistical approach, *Ceram. Int.*, 2012, **38**, 6753.

32 A. Witek-Krowiak, K. Chojnacka, D. Podstawczyk, A. Dawiec and K. Pokomeda, Application of response surface methodology and artificial neural networks method in modelling and optimization of biosorption process, *Bioresour. Technol.*, 2014, **160**, 150.

33 K. Anupam, S. Dutta, C. Bhattacharjee and S. Datta, Adsorptive removal of chromium(VI) from aqueous solution over powder activated carbon: optimization through response surface methodology, *Chem. Eng. J.*, 2011, **173**, 135.

34 K. Kalantari, M. B. Ahmad, H. R. F. Masoumi, K. Shameli, M. Basri and R. Khandanloum, Rapid and high capacity adsorption of heavy metals by Fe_3O_4/montmorillonite nanocomposite using response surface methodology: preparation, characterization, optimization, equilibrium isotherms and adsorption kinetics study, *J. Taiwan Inst. Chem. Eng.*, 2014, **49**, 192.

35 H. Chaair, J. C. Heughebaert, M. Heughebaert and M. Vaillant, Statistical analysis of apatitic tricalcium phosphate preparation, *J. Mater. Chem.*, 1994, **4**, 765.

36 T. S. Anirudhan and M. Ramachandran, Adsorptive removal of tannin from aqueous solutions by cationic surfactant-modified bentonite clay, *J. Colloid Interface Sci.*, 2006, **299**, 116.

37 B. Mohammed, D. Amina and G. Samira, The dicalcium phosphate dihydrate fixator and stabilizer of glutaraldehyde, *Mater. Sci. Eng., B*, 2013, **3**, 605.

38 A. B. Đukić, K. R. Kumrić, N. S. Vukelić, Z. S. Stojanović, M. D. Stojmenović, S. S. Milošević and L. L. Matović, Influence of ageing of milled clay and its composite with TiO_2 on the heavy metal adsorption characteristics, *Ceram. Int.*, 2015, **41**, 5129.

39 M. Danish, R. Hashim, M. Rafatullah, O. Sulaiman, A. Ahmad and Govind, Adsorption of lead(II) ions from aqueous solutions by date bead carbon activated with $ZnCl_2$, *Clean: Soil, Air, Water*, 2011, **39**, 392.

40 Y. Sag and Y. Aktay, Mass transfer and equilibrium studies for the sorption of chromium ions onto chitin, *Process Biochem.*, 2000, **36**, 157.

41 F. Ayari, E. Srasra and M. Trabelsi- Ayadi, Retension of lead from an aqueous solution by use of bentonite as adsorbent for reducing leaching from industrial effluents, *Desalination*, 2007, **206**, 270.

42 P. Chand and Y. B. Pakade, Synthesis and characterization of hydroxyapatite nanoparticles impregnated on apple pomace to enhance adsorption of Pb(II), Cd(II) and Ni(II) ions from aqueous solution, *Environ. Sci. Pollut. Res.*, 2015, **22**, 10919.

43 C. H. Liu, Y. H. Chuang, T. Y. Chen, Y. Tian, H. Li, M. K. Wang and W. Zhang, Mechanism of arsenic adsorption on magnetite nanoparticles from water: thermodynamic and spectroscopic studies, *Environ. Sci. Technol.*, 2015, **49**, 7726.

44 J. Wang, G. Liu, T. Li and C. Zhou, Physicochemical studies toward the removal of Zn(II) and Pb(II) through adsorption on montmorillonite-supported zero-valent iron nanoparticles, *RSC Adv.*, 2015, **5**, 29859.

45 M. S. Fernando, R. M. De Silva and K. M. N. de Silva, Synthesis, characterization, and application of nano hydroxyapatite and nanocomposite of hydroxyapatite with granular activated carbon for the removal of Pb^{2+} from aqueous solutions, *Appl. Surf. Sci.*, 2015, **351**, 95.

46 S. Saadat, A. K. Jashni and M. M. Doroodmand, Synthesis and characterization of novel single-walled carbon nanotubes- doped walnut shell composite and its adsorption performance for lead in aqueous solutions, *J. Environ. Chem. Eng.*, 2014, **2**, 2059.

47 L. Yang, Z. Li, G. Nie, Z. Zhang and X. Lu, Fabrication of poly(*o*-phenylenediamine)/reduced graphene oxide composite nanosheets *via* microwave heating and their effective adsorption of lead ions, *Appl. Surf. Sci.*, 2014, **307**, 601.

48 R. D. C. Soltani, G. S. Khorramabadi, A. R. Khataee and S. Jorfi, Silica nanopowders/alginate composite for adsorption of lead(II) ions in aqueous solutions, *J. Taiwan Inst. Chem. Eng.*, 2014, **45**, 973.

49 A. Dhillon and D. Kumar, Development of nanoporous adsorbent for the removal of health-hazardous fluoride ions from aqueous system, *J. Mater. Chem. A*, 2015, **3**, 4215.

50 Y. Ren, N. Yan, J. Feng, J. Ma, Q. Wen, N. Li and Q. Dong, Adsorption mechanism of copper and lead ions onto graphene nanosheet/δ-MnO_2, *Mater. Chem. Phys.*, 2012, **136**, 538.

51 L. Deng, Y. Su, H. Su, X. Wang and X. Zhu, Sorption and desorption of lead(II) from wastewater by green algae *Cladophora fascicularis*, *J. Hazard. Mater.*, 2007, **143**, 220–225.

